

The spherical harmonic representation of the gravitational field quantities generated by the ice density contrast

Robert TENZER¹, Ahmed ABDALLA¹, Peter VAJDA², HAMAYUN³

¹ National School of Surveying, Division of Sciences, University of Otago
310 Castle Street, Dunedin, New Zealand; e-mail: robert.tenzer@surveying.otago.ac.nz

² Geophysical Institute of the Slovak Academy of Sciences
Dúbravská cesta 9, 845 28 Bratislava, Slovak Republic; e-mail: Peter.Vajda@savba.sk

³ Delft Institute of Earth Observation and Space Systems (DEOS)
Delft University of Technology, Kluyverweg 1, 2629 HS Delft, The Netherlands; e-mail: K.Hamayun@tudelft.nl

Abstract: We derive the expressions for computing the ice density contrast stripping corrections to the topography corrected gravity field quantities by means of the spherical harmonics. The expressions in the spectral representation utilize two types of the spherical functions, namely the spherical height functions and the newly introduced lower-bound ice functions. The spherical height functions describe the global geometry of the upper topographic bound. The spherical lower-bound ice functions combined with the spherical height functions describe the global thickness of the continental ice sheet. The newly derived formulas are utilized in the forward modelling of the gravitational field quantities generated by the ice density contrast. The 30×30 arc-sec global elevation data from GTOPO30 are used to generate the global elevation model (GEM) coefficients. The spatially averaged global elevation data from GTOPO30 and the 2×2 arc-deg ice-thickness data from the CRUST 2.0 global crustal model are used to generate the global lower-bound ice model (GIM) coefficients. The mean value of the ice density contrast 1753 kg/m^3 (i.e., difference of the reference constant density of the continental upper crust 2670 kg/m^3 and the density of glacial ice 917 kg/m^3) is adopted. The numerical examples are given for the gravitational potential and attraction generated by the ice density contrast computed globally with a low-degree spectral resolution complete to degree and order 90 of the GEM and GIM coefficients.

Key words: correction, density, gravity, ice, spherical harmonics

1. Introduction

The global geopotential and elevation models are currently available to a very high accuracy and resolution. On the contrary, the accurate modelling of the topography corrected gravity field quantities is restricted by the current lack of knowledge about the density distribution within the upper continental crust. The constant average topographic density is thus commonly assumed when modelling the topographic corrections to gravity field quantities evaluated with a low-degree spectral resolution (e.g., *Sünkel, 1968; Novák et al., 2001; Tenzer et al., 2003; Novák and Grafarend, 2005*). Recently, the lateral topographical density distribution models have been used more often in detailed gravimetric modelling at the vicinity of the computation point, whereas the constant average topographical density is adopted for computing the gravitational contribution of the far-zone topography (e.g., *Martinec et al., 1995; Kühtreiber, 1998; Huang et al., 2001; Hunegnaw, 2001; Sjöberg, 2004*). Nevertheless, the effect of the anomalous density variations within the far-zone topography due to the large-scale sedimentary basins and continental ice sheet is still significant. Similarly, the large-scale geological formations with variable density structures within the upper continental crust contribute considerably to the long-wavelength part of the topography corrected gravity field. It is thus expected that the incorporation of the currently available ice, sediment, and crust density contrasts data from the global crustal model CRUST 2.0 (*Bassin et al., 2000*) could improve the accuracy of modelling the topography corrected gravity field quantities, particularly in polar regions and over areas with the large-scale sedimentary basins and other geological formations with variable density structures.

A number of authors utilized the spherical harmonic analysis in deriving the expressions for computing the atmospheric and topographic corrections to gravity field quantities. A brief summary of these studies can be found for instance in *Tenzer et al. (2010)*. *Ramillien (2002)*, *Tenzer et al. (2009c)*, and others computed globally the atmospheric corrections using methods for a spherical harmonic analysis of gravity field. The expressions for computing the bathymetric stripping corrections by means of spherical harmonics were derived by *Novák (2010)* and *Tenzer et al. (2010)*. The stripping corrections to gravity field quantities due to the major known density contrasts within

the Earth's crust were systematically investigated and computed globally with a low-degree spectral resolution in *Tenzer et al. (2008a, 2008b, 2009a, 2009b)* using the CRUST 2.0 global crustal model.

In this study, we derive the expressions for computing the ice density contrast stripping corrections to gravity field quantities by means of spherical harmonics. The thickness of the polar ice sheet is described by the global elevation model (GEM) coefficients and the global lower-bound ice model (GIM) coefficients. The gravitational potential generated by the ice density contrast and the respective gravitational attraction are formulated in terms of the spherical height and lower-bound ice functions in Section 2. The GEM and GIM coefficients are used to compute globally the long-wavelength gravitational potential and attraction with a spectral resolution complete to degree 90 of spherical harmonics. The GTOPO30 global elevation and CRUST 2.0 ice-thickness data are used to generate the GEM and GIM coefficients. The numerical examples are shown in Section 3. The summary and conclusions are given in Section 4.

2. Spectral representation of the ice stripping gravity corrections

Adopting the spherical approximation of the Earth's shape, the gravitational potential generated by the ice density contrast V^{ice} computed at the position (r, Ω) is defined by Newton's volume integral in the following form

$$V^{ice}(r, \Omega) = G \Delta\rho^{ice} \iint_{\Phi} \int_{R+L(\Omega')}^{R+H(\Omega')} \ell^{-1}(r, \psi, r') r'^2 dr' d\Omega', \quad (1)$$

where G is Newton's gravitational constant, H the height above sea level, L the vertical displacement of the lower ice bound measured from sea level, ℓ the Euclidean spatial distance between two points (r, Ω) and (r', Ω') , ψ the spherical distance, $d\Omega = \sin\phi d\phi d\lambda$ the infinitesimal surface element on the unit sphere, and $\Phi = \{ \Omega = (\phi, \lambda) : \phi \in [-\pi/2, \pi/2] \wedge \lambda \in [0, 2\pi) \}$. The geocentric radius of the geoid surface is approximated by the Earth's mean radius R . The 3-D position is defined by the geocentric spherical coordinates (r, ϕ, λ) , where r is the geocentric radius and $\Omega = (\phi, \lambda)$ denotes the geocentric direction with the geocentric spherical latitude ϕ and longitude

λ . The constant value of the ice density contrast $\Delta\rho^{\text{ice}}$ in Eq. (1) is defined as the difference of the reference density of the continental upper crust ρ^t and the density of glacial ice ρ^{ice} . The density volume of the polar ice sheet is enclosed between the upper and lower ice bounds. The upper ice bound is identical with the upper topographic bound over the areas of the polar ice sheet. The vertical displacement between the upper topographic bound and the lower ice bound then equals zero everywhere outside the areas covered by the polar ice sheet.

To derive the expressions for computing the gravitational field quantities generated by the ice density contrast in the spectral representation, the gravitational potential V^{ice} in Eq. (1) is first rewritten as

$$\begin{aligned}
 V^{\text{ice}}(r, \Omega) = & G \Delta\rho^{\text{ice}} \iint_{\Phi} \int_R^{R+H(\Omega')} \ell^{-1}(r, \psi, r') r'^2 dr' d\Omega' - \\
 & - G \Delta\rho^{\text{ice}} \iint_{\Phi} \int_R^{R+L(\Omega')} \ell^{-1}(r, \psi, r') r'^2 dr' d\Omega'. \tag{2}
 \end{aligned}$$

The first term on the right-hand side of Eq. (2) represents the gravitational contribution of the masses enclosed between the upper topographic bound and the reference sphere of radius R . The second term represents the gravitational contribution of the masses enclosed between the lower ice bound and the reference sphere of radius R . The difference of these two gravitational contributions gives the gravitational contribution of the ice density contrast enclosed between the upper topographic bound and the lower ice bound.

With reference to the Legendre addition theorem (e.g., *Novotný, 1982*), the reciprocal spatial distance ℓ^{-1} in Eq. (2) is expanded into an infinite series of the spherical harmonics. For the external convergence domain $r \geq r'$, the series reads

$$\ell^{-1}(r, \psi, r') = \frac{1}{r} \sum_{n=0}^{\infty} \sum_{m=-n}^n \frac{1}{2n+1} \left(\frac{r'}{r}\right)^n Y_{n,m}(\Omega) Y_{n,m}^*(\Omega'), \tag{3}$$

where $Y_{n,m}(\Omega)$ and $Y_{n,m}^*(\Omega')$ are the surface spherical harmonic functions and their complex conjugates, respectively (cf., *Abramowitz and Stegun, 1972*). The series in Eq. (3) is uniformly convergent for $r \geq r'$. Substituting

from Eq. (3) to Eq. (2), we get

$$\begin{aligned}
 V^{\text{ice}}(r, \Omega) = & G \Delta \rho^{\text{ice}} \sum_{n=0}^{\infty} \sum_{m=-n}^n \left(\frac{1}{r}\right)^{n+1} \frac{1}{2n+1} Y_{n,m}(\Omega) \iint_{\Phi} Y_{n,m}^*(\Omega') \times \\
 & \times \int_{\mathbb{R}}^{\mathbb{R}+H(\Omega')} r'^{n+2} dr' d\Omega' - G \Delta \rho^{\text{ice}} \sum_{n=0}^{\infty} \sum_{m=-n}^n \left(\frac{1}{r}\right)^{n+1} \times \\
 & \times \frac{1}{2n+1} Y_{n,m}(\Omega) \iint_{\Phi} Y_{n,m}^*(\Omega') \int_{\mathbb{R}}^{\mathbb{R}+L(\Omega')} + r'^{n+2} dr' d\Omega'. \tag{4}
 \end{aligned}$$

Since the expansion of Newton’s integral kernel into a series of the spherical harmonic functions converges uniformly when computed for a point located outside the gravitating masses, the interchange of summation and integration in Eq. (4) is permissible (cf., *Moritz, 1980*). The radial integral in the first constituent on the right-hand side of Eq. (4) is evaluated as (cf., *Tsouliis, 1999, 2001*; see also *Novák, 2010*, Eqs. 11 and 12)

$$\int_{\mathbb{R}}^{\mathbb{R}+H(\Omega)} r^{n+2} dr = \frac{\mathbb{R}^{n+3}}{n+3} \sum_{k=1}^{n+3} \binom{n+3}{k} \left(\frac{H}{\mathbb{R}}\right)^k = \mathbb{R}^{n+3} F^t(\Omega), \tag{5}$$

with the following substitution

$$F^t(\Omega) \approx \frac{H(\Omega)}{\mathbb{R}} + (n+2) \frac{H^2(\Omega)}{2\mathbb{R}^2} + (n+2)(n+1) \frac{H^3(\Omega)}{6\mathbb{R}^3}. \tag{6}$$

The spectral representation of the function F^t in Eq. (5) is defined as (cf., *Novák, 2010*)

$$F^t(\Omega) = \sum_{n=0}^{\infty} \sum_{m=-n}^n F_{n,m}^t Y_{n,m}(\Omega). \tag{7}$$

The numerical coefficients $F_{n,m}^t$ in Eq. (7) read

$$F_{n,m}^t \approx \frac{H_{n,m}}{\mathbb{R}} + (n+2) \frac{H_{n,m}^{(2)}}{2\mathbb{R}^2} + (n+2)(n+1) \frac{H_{n,m}^{(3)}}{6\mathbb{R}^3}, \tag{8}$$

where $H_{n,m}$ are the GEM coefficients of degree n and order m . The definition of the coefficients $H_{n,m}$, $H_{n,m}^{(2)}$ and $H_{n,m}^{(3)}$ is given in Eqs. (17–19).

By analogy with Eq. (5), the radial integral in the second constituent on the right-hand side of Eq. (4) is evaluated as

$$\int_{\mathbb{R}}^{\mathbb{R}+L(\Omega)} r^{n+2} dr = \frac{\mathbb{R}^{n+3}}{n+3} \sum_{k=1}^{n+3} \binom{n+3}{k} \left(\frac{L}{\mathbb{R}}\right)^k = \mathbb{R}^{n+3} F^L(\Omega), \tag{9}$$

where the function F^L reads

$$F^L(\Omega) \approx \frac{L(\Omega)}{\mathbb{R}} + (n+2) \frac{L^2(\Omega)}{2\mathbb{R}^2} + (n+2)(n+1) \frac{L^3(\Omega)}{6\mathbb{R}^3}. \tag{10}$$

The spectral representation of the function F^L is introduced in the following form

$$F^L(\Omega) = \sum_{n=0}^{\infty} \sum_{m=-n}^n F_{n,m}^L Y_{n,m}(\Omega). \tag{11}$$

The numerical coefficients $F_{n,m}^L$ in Eq. (11) are given by

$$F_{n,m}^L \approx \frac{L_{n,m}}{\mathbb{R}} + (n+2) \frac{L_{n,m}^{(2)}}{2\mathbb{R}^2} + (n+2)(n+1) \frac{L_{n,m}^{(3)}}{6\mathbb{R}^3}, \tag{12}$$

where $L_{n,m}$ are the GIM coefficients of degree n and order m . The definition of the coefficients $L_{n,m}$, $L_{n,m}^{(2)}$ and $L_{n,m}^{(3)}$ is given in Eqs. (20–22).

Inserting from Eqs. (5) and (9) to Eq. (4), the gravitational potential V^{ice} becomes

$$\begin{aligned} V^{\text{ice}}(r, \Omega) = & \text{GR}^2 \Delta\rho^{\text{ice}} \sum_{n=0}^{\bar{n}} \sum_{m=-n}^n \left(\frac{\mathbb{R}}{r}\right)^{n+1} \frac{1}{2n+1} Y_{n,m}(\Omega) \iint_{\Phi} F^t(\Omega') \times \\ & \times Y_{n,m}^*(\Omega') d\Omega' - \text{GR}^2 \Delta\rho^{\text{ice}} \sum_{n=0}^{\bar{n}} \sum_{m=-n}^n \left(\frac{\mathbb{R}}{r}\right)^{n+1} \times \\ & \times \frac{1}{2n+1} Y_{n,m}(\Omega) \iint_{\Phi} F^L(\Omega') Y_{n,m}^*(\Omega') d\Omega', \end{aligned} \tag{13}$$

where \bar{n} is the maximum degree of spherical harmonics. The substitution from Eqs. (7) and (11) to Eq. (13) further yields

$$\begin{aligned} V^{\text{ice}}(r, \Omega) = & \text{GR}^2 \Delta\rho^{\text{ice}} \sum_{n=0}^{\bar{n}} \sum_{m=-n}^n \left(\frac{\mathbb{R}}{r}\right)^{n+1} \frac{1}{2n+1} Y_{n,m}(\Omega) \times \\ & \times \sum_{n'=0}^{\bar{n}'} \sum_{m'=-n'}^{n'} F_{n',m'}^t \iint_{\Phi} Y_{n',m'}(\Omega') Y_{n,m}^*(\Omega') d\Omega' - \end{aligned}$$

$$\begin{aligned}
 & - \text{GR}^2 \Delta \rho^{\text{ice}} \sum_{n=0}^{\bar{n}} \sum_{m=-n}^n \left(\frac{\text{R}}{r}\right)^{n+1} \frac{1}{2n+1} Y_{n,m}(\Omega) \times \\
 & \times \sum_{n'=0}^{\bar{n}'} \sum_{m'=-n'}^{n'} F_{n',m'}^{\text{L}} \iint_{\Phi} Y_{n',m'}(\Omega') Y_{n,m}^*(\Omega') d\Omega'. \tag{14}
 \end{aligned}$$

Taking into account the orthogonality property of the spherical harmonic functions, i.e.,

$$\iint_{\Phi} Y_{n',m'}(\Omega') Y_{n,m}^*(\Omega') d\Omega' = 4\pi \delta_{n,n'} \delta_{m,m'} \quad ,$$

where

$$\delta_{n,n'} = \begin{cases} 1 & \text{for } n = n' \\ 0 & \text{for } n \neq n' \end{cases} \quad , \quad \delta_{m,m'} = \begin{cases} 1 & \text{for } m = m' \\ 0 & \text{for } m \neq m' \end{cases} \quad ,$$

the gravitational potential V^{ice} in Eq. (14) takes the following form

$$\begin{aligned}
 V^{\text{ice}}(r, \Omega) &= 4\pi \text{GR}^2 \Delta \rho^{\text{ice}} \sum_{n=0}^{\bar{n}} \sum_{m=-n}^n \left(\frac{\text{R}}{r}\right)^{n+1} \frac{1}{2n+1} F_{n,m}^{\text{t}} Y_{n,m}(\Omega) - \\
 & - 4\pi \text{GR}^2 \Delta \rho^{\text{ice}} \sum_{n=0}^{\bar{n}} \sum_{m=-n}^n \left(\frac{\text{R}}{r}\right)^{n+1} \frac{1}{2n+1} F_{n,m}^{\text{L}} Y_{n,m}(\Omega) = \\
 & = 4\pi \text{GR}^2 \Delta \rho^{\text{ice}} \sum_{n=0}^{\bar{n}} \sum_{m=-n}^n \left(\frac{\text{R}}{r}\right)^{n+1} \frac{1}{2n+1} (F_{n,m}^{\text{t}} - F_{n,m}^{\text{L}}) Y_{n,m}(\Omega). \tag{15}
 \end{aligned}$$

Inserting from Eqs. (8) and (12) to Eq. (15), we arrive at

$$\begin{aligned}
 V^{\text{ice}}(r, \Omega) &\approx 4\pi \text{GR} \Delta \rho^{\text{ice}} \sum_{n=0}^{\bar{n}} \left(\frac{\text{R}}{r}\right)^{n+1} \frac{1}{2n+1} \sum_{m=-n}^n (H_{n,m} - L_{n,m}) \times \\
 & \times Y_{n,m}(\Omega) + 2\pi \text{G} \Delta \rho^{\text{ice}} \sum_{n=0}^{\bar{n}} \left(\frac{\text{R}}{r}\right)^{n+1} \frac{n+2}{2n+1} \sum_{m=-n}^n (H_{n,m}^{(2)} - L_{n,m}^{(2)}) \times \\
 & \times Y_{n,m}(\Omega) + \frac{2}{3\text{R}} \pi \text{G} \Delta \rho^{\text{ice}} \sum_{n=0}^{\bar{n}} \left(\frac{\text{R}}{r}\right)^{n+1} \frac{(n+2)(n+1)}{2n+1} \times \\
 & \times \sum_{m=-n}^n (H_{n,m}^{(3)} - L_{n,m}^{(3)}) Y_{n,m}(\Omega). \tag{16}
 \end{aligned}$$

The series in eqn. (16) is convergent for the maximum degree of spherical harmonics $\bar{n} = 90$ used for a numerical realization in Section 3. When increasing the maximum degree of spherical harmonics above this limit, the series in eqn. (16) can become divergent. The analysis of the convergence domain is thus essential for finding an optimal truncation degree of the functions F^t and F^L in Eqs. (6) and (10). The convergence and optimal truncation of binomial series were studied by *Rummel et al.* (1988) and *Sun and Sjöberg* (2001). The higher-degree terms of the expression for computing the gravitational potential generated by the ice density contrast in Eq. (16) can be obtained from the binomial series for $k > 3$ in Eqs. (5) and (9). The term $\sum_{m=-n}^n H_{n,m} Y_{n,m}(\Omega)$ in Eq. (16) defines the spherical height function $H_n(\Omega)$ of degree n (see e.g., *Novák et al., 2001*). It reads

$$H_n(\Omega) = \frac{2n + 1}{4\pi} \iint_{\Phi} H(\Omega') P_n(\cos \psi) d\Omega' = \sum_{m=-n}^n H_{n,m} Y_{n,m}(\Omega), \quad (17)$$

where P_n is the Legendre polynomial of degree n for the argument of the spherical distance ψ . Consequently, $H_n^{(2)}(\Omega)$ and $H_n^{(3)}(\Omega)$ are defined as follows (*ibid.*)

$$H_n^{(2)}(\Omega) = \frac{2n + 1}{4\pi} \iint_{\Phi} H^2(\Omega') P_n(\cos \psi) d\Omega' = \sum_{m=-n}^n H_{n,m}^{(2)} Y_{n,m}(\Omega), \quad (18)$$

$$H_n^{(3)}(\Omega) = \frac{2n + 1}{4\pi} \iint_{\Phi} H^3(\Omega') P_n(\cos \psi) d\Omega' = \sum_{m=-n}^n H_{n,m}^{(3)} Y_{n,m}(\Omega). \quad (19)$$

Similarly, we introduce the spherical lower-bound ice functions $L_n(\Omega)$ in the following form

$$\begin{aligned} L_n(\Omega) &= \frac{2n + 1}{4\pi} \iint_{\Phi} [H(\Omega') - I(\Omega')] P_n(\cos \psi) d\Omega' = \\ &= \sum_{m=-n}^n L_{n,m} Y_{n,m}(\Omega). \end{aligned} \quad (20)$$

The corresponding functions $L_n^{(2)}(\Omega)$ and $L_n^{(3)}(\Omega)$ read

$$\begin{aligned}
 L_n^{(2)}(\Omega) &= \frac{2n+1}{4\pi} \iint_{\Phi} [H(\Omega') - I(\Omega')]^2 P_n(\cos\psi) d\Omega' = \\
 &= \sum_{m=-n}^n L_{n,m}^{(2)} Y_{n,m}(\Omega), \tag{21}
 \end{aligned}$$

$$\begin{aligned}
 L_n^{(3)}(\Omega) &= \frac{2n+1}{4\pi} \iint_{\Phi} [H(\Omega') - I(\Omega')]^3 P_n(\cos\psi) d\Omega' = \\
 &= \sum_{m=-n}^n L_{n,m}^{(3)} Y_{n,m}(\Omega). \tag{22}
 \end{aligned}$$

The lower ice bound L in Eqs. (20–22) is defined as the difference of the height H and the ice thickness I . The GIM coefficients $L_{n,m}$ can then be computed from available global elevation and ice-thickness data.

The substitutions of the spherical height functions from Eqs. (17–19) and of the spherical lower-bound ice functions from Eqs. (20–22) to Eq. (16) yield

$$\begin{aligned}
 V^{\text{ice}}(r, \Omega) &= 4\pi GR \Delta\rho^{\text{ice}} \sum_{n=0}^{\bar{n}} \left(\frac{R}{r}\right)^{n+1} \frac{1}{2n+1} [H_n(\Omega) - L_n(\Omega)] + \\
 &+ 2\pi G \Delta\rho^{\text{ice}} \sum_{n=0}^{\bar{n}} \left(\frac{R}{r}\right)^{n+1} \frac{n+2}{2n+1} [H_n^{(2)}(\Omega) - L_n^{(2)}(\Omega)] + \\
 &+ \frac{2}{3R} \pi G \Delta\rho^{\text{ice}} \sum_{n=0}^{\bar{n}} \left(\frac{R}{r}\right)^{n+1} \frac{(n+2)(n+1)}{2n+1} [H_n^{(3)}(\Omega) - L_n^{(3)}(\Omega)]. \tag{23}
 \end{aligned}$$

The gravitational attraction generated by the ice density contrast g^{ice} is approximately defined as a negative radial derivative of the respective gravitational potential V^{ice} (e.g., *Martinec, 1998*)

$$\begin{aligned}
 g^{\text{ice}}(r, \Omega) &\cong -\frac{\partial V^{\text{ice}}(r, \Omega)}{\partial r} = \\
 &= -G \Delta\rho^{\text{ice}} \iint_{\Phi} \int_{R+L(\Omega')}^{R+H(\Omega')} \frac{\partial \ell^{-1}(r, \psi, r')}{\partial r} r'^2 dr' d\Omega' =
 \end{aligned}$$

$$\begin{aligned}
 &= -G \Delta \rho^{\text{ice}} \iint_{\Phi} \int_{\mathbb{R}}^{\mathbb{R}+H(\Omega')} \frac{\partial \ell^{-1}(r, \psi, r')}{\partial r} r'^2 dr' d\Omega' + \\
 &+ G \Delta \rho^{\text{ice}} \iint_{\Phi} \int_{\mathbb{R}}^{\mathbb{R}+L(\Omega')} \frac{\partial \ell^{-1}(r, \psi, r')}{\partial r} r'^2 dr' d\Omega'. \tag{24}
 \end{aligned}$$

From Eqs. (23) and (24), the gravitational attraction g^{ice} is found to be

$$\begin{aligned}
 g^{\text{ice}}(r, \Omega) &= 4\pi G \Delta \rho^{\text{ice}} \sum_{n=0}^{\bar{n}} \left(\frac{\mathbb{R}}{r}\right)^{n+2} \frac{n+1}{2n+1} [H_n(\Omega) - L_n(\Omega)] + \\
 &+ \frac{2}{\mathbb{R}} \pi G \Delta \rho^{\text{ice}} \sum_{n=0}^{\bar{n}} \left(\frac{\mathbb{R}}{r}\right)^{n+2} \frac{(n+2)(n+1)}{2n+1} [H_n^{(2)}(\Omega) - L_n^{(2)}(\Omega)] + \\
 &+ \frac{2}{3\mathbb{R}^2} \pi G \Delta \rho^{\text{ice}} \sum_{n=0}^{\bar{n}} \left(\frac{\mathbb{R}}{r}\right)^{n+2} \frac{(n+2)(n+1)^2}{2n+1} [H_n^{(3)}(\Omega) - L_n^{(3)}(\Omega)]. \tag{25}
 \end{aligned}$$

By analogy with Eq. (16), Eq. (25) is finally rewritten as

$$\begin{aligned}
 g^{\text{ice}}(r, \Omega) &= 4\pi G \Delta \rho^{\text{ice}} \sum_{n=0}^{\bar{n}} \left(\frac{\mathbb{R}}{r}\right)^{n+2} \frac{n+1}{2n+1} \times \\
 &\times \sum_{m=-n}^n (H_{n,m} - L_{n,m}) Y_{n,m}(\Omega) + \frac{2}{\mathbb{R}} \pi G \Delta \rho^{\text{ice}} \times \\
 &\times \sum_{n=0}^{\bar{n}} \left(\frac{\mathbb{R}}{r}\right)^{n+2} \frac{(n+2)(n+1)}{2n+1} \sum_{m=-n}^n (H_{n,m}^{(2)} - L_{n,m}^{(2)}) Y_{n,m}(\Omega) + \\
 &+ \frac{2}{3\mathbb{R}^2} \pi G \Delta \rho^{\text{ice}} \sum_{n=0}^{\bar{n}} \left(\frac{\mathbb{R}}{r}\right)^{n+2} \frac{(n+2)(n+1)^2}{2n+1} \times \\
 &\times \sum_{m=-n}^n (H_{n,m}^{(3)} - L_{n,m}^{(3)}) Y_{n,m}(\Omega). \tag{26}
 \end{aligned}$$

We note here that the expressions for computing the gravitational field quantities generated by the ice density contrast in Eqs. (16) and (26) can be reformulated for the ellipsoidal approximation of the Earth’s shape according to the approach described in *Vaniček et al. (1995)*. Alternatively,

these expressions can directly be formulated by means of the ellipsoidal harmonics.

3. Numerical examples

The 30×30 arc-sec global elevation data from the GTOPO30 model (provided by the US Geological Survey's EROS Data Center) are used to generate the GEM coefficients. The 2×2 arc-deg mean heights computed by spatial averaging of the 30×30 arc-sec global elevation data from GTOPO30 and the discrete data of the ice thickness with a 2×2 arc-deg geographical resolution from the CRUST 2.0 global crustal model are used to generate the GIM coefficients. The 2×2 arc-deg discrete data of the ice thickness from the CRUST 2.0 model are shown in Fig. 1. The maxima of the ice thickness reach ~ 4 km.

The newly derived expressions in Eqs. (16) and (26) are utilized in the

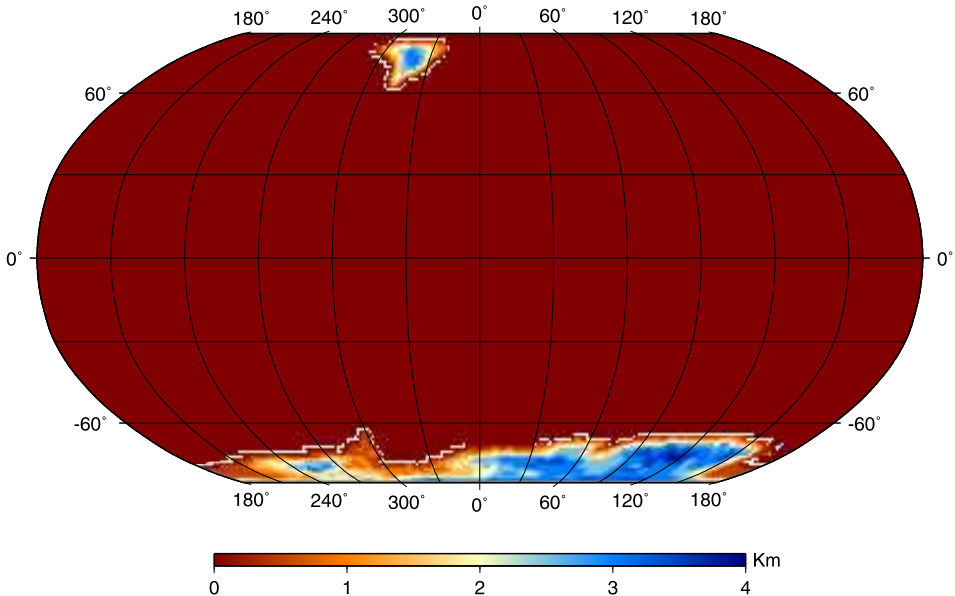


Fig. 1. The 2×2 arc-deg discrete data of the ice thickness from the CRUST 2.0 global crustal model.

forward modelling of the gravitational potential and attraction generated by the ice density contrast. The mean value of the ice density contrast 1753 kg/m^3 is adopted. This value of the ice density contrast is obtained as the difference of the reference density of the continental upper crust 2670 kg/m^3 (cf., *Hinze, 2003*) and the density of glacial ice 917 kg/m^3 (cf. e.g., *Cutnell and Kenneth, 1995*). The gravitational potential and attraction are computed with a spectral resolution complete to degree and order 90 of the GEM and GIM coefficients. The computation is realized globally on a 1×1 arc-deg geographical grid at the Earth’s surface. The results are shown in Figs. 2 and 3. The computed gravitational potential generated by the ice density contrast varies from 320 to $3496 \text{ m}^2\text{s}^{-2}$ with the mean of $742 \text{ m}^2\text{s}^{-2}$, and the standard deviation is $734 \text{ m}^2\text{s}^{-2}$. Its maxima are located in the central and eastern Antarctica. The computed gravitational attraction generated by the ice density contrast varies from 3 to 301 mGal with the mean of 22 mGal, and the standard deviation is 55 mGal. Its maxima

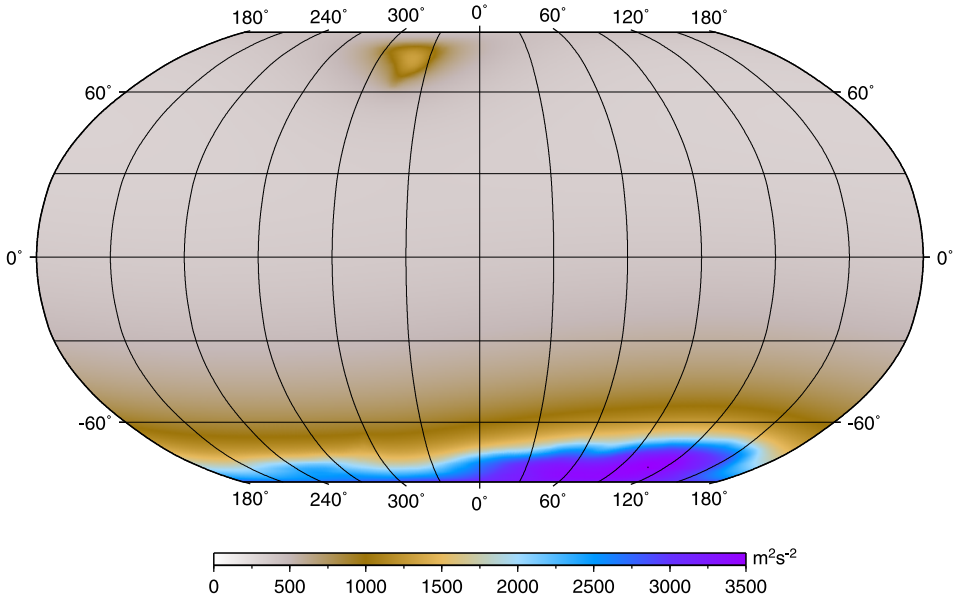


Fig. 2. The gravitational potential generated by the ice density contrast (1753 kg/m^3) computed on a 1×1 arc-deg grid at the Earth’s surface using the GEM and GIM coefficients complete to degree and order 90.

are located throughout regions with the largest continental ice thickness in the central Greenland and the central and eastern Antarctica. The ice density contrast stripping correction was applied to the topography corrected gravity disturbances in *Tenzer et al. (2009b)*. The ice density contrast stripping corrections to the topography corrected gravity anomalies and geoid undulations were investigated in *Tenzer et al. (2009a, 2008b)*. The results of these studies revealed that the ice density contrast stripping corrections significantly changed the topography corrected gravity field quantities over the regions with a large thickness of the continental ice sheet in Greenland and Antarctica.

The largest errors in computed gravitational field quantities generated by the ice density contrast are due to inaccuracies within the currently available ice-thickness data of the CRUST 2.0 global crustal model and consequently in computed numerical values of the GIM coefficients which describe the

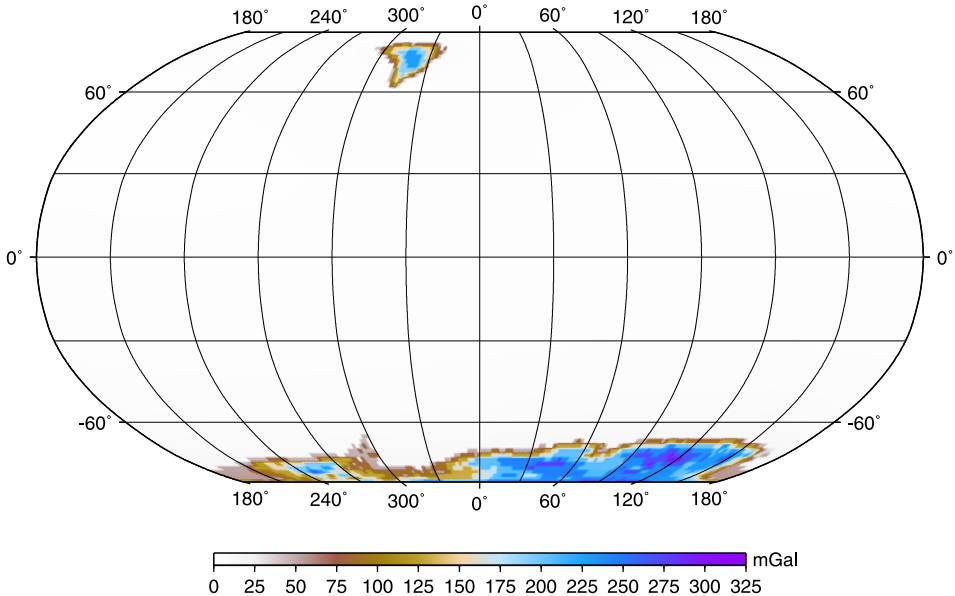


Fig. 3. The gravitational attraction generated by the ice density contrast (1753 kg/m^3) computed on a 1×1 arc-deg grid at the Earth's surface using the GEM and GIM coefficients complete to degree and order 90.

global geometry of the lower ice bound. The global geometry of the upper ice bound is described to a very high accuracy and resolution by the GEM coefficients generated from the currently available global elevation data. The relative errors in computed gravity field quantities due to adopting the constant density of glacial ice (917 kg/m^3) mainly depend on the ratio of the firn ice layer and the consolidated glacial ice over the areas covered by the continental ice sheet. The contribution of the sea ice density which has large seasonal variations is not taken into consideration; the reported values of the sea ice density vary over a wide range from about 720 to 940 kg/m^3 , with an average of approximately 910 kg/m^3 (see e.g., *Timco and Frederking, 1996*). The vertical structure of the continental ice sheet consists of three layers formed by the snow, firn ice and consolidated glacial ice. The firn ice represents the intermediate stage between fresh snow and glacial ice, and has a density between that of the surface snow (in Greenland and Antarctica typically to about 350 kg/m^3) and glacial ice (typically 917 kg/m^3). In the absence of significant melting, the ice firn densification rate depends mainly on snow temperature, burial rate (surface accumulation) and near-surface wind speed. Below the depth of approximately 15 m , densification occurs at constant temperature equal to the annual mean surface temperature (cf., *van den Broeke, 2008*). The spatial variability of the depth and density of the Antarctic and Greenland ice firn layer varies significantly depending on the numerous climatic and near-surface atmospheric factors. At the South Pole, for instance, the densification is slow, and the firn-layer thickness exceeds 100 m . A typical thickness of the ice firn layer is about 70 to 100 m . In regions with active katabatic winds and low precipitation rates, the firn layer may have been completely removed by snowdrift erosion and/or sublimation, exposing the glacier ice at the surface. The lower density within the ice firn layer comparing to the density of the glacial ice can be accounted for by reducing the total thickness of the ice sheet not more than 20 to 25 m . The errors in computed gravitational field quantities generated by the ice density contrast due to the density variations within the ice sheet are thus completely negligible comparing to the errors due to uncertainties of the CRUST 2.0 ice-thickness data used in this study. The forward modelling of the ice density contrast stripping corrections with a higher accuracy and resolution requires the facilitation of the 10×10 arc-min global ice thickness data from the ICE-5G (VM2) model (see *Peltier, 2004*).

4. Summary and conclusions

We have derived the expressions in terms of the spherical height and lower-bound ice functions for computing the ice density contrast stripping corrections to the topography corrected gravity field quantities. These two types of the spherical functions describe the global thickness of the polar ice sheet.

The newly derived formulas were utilized in the forward modelling of the gravitational field quantities generated by the ice density contrast. The numerical examples were given for the gravitational potential and attraction computed globally with a low-degree spectral resolution complete to degree and order 90 of the GEM and GIM coefficients. The GEM and GIM coefficients were generated from the GTOPO30 global elevation and CRUST 2.0 ice-thickness data.

The results revealed that the maxima of the gravitational potential generated by the ice density contrast reach $\sim 3500 \text{ m}^2 \text{ s}^{-2}$ in the regions with the largest thickness of the Greenland and Antarctic continental ice sheets. The maxima of the corresponding gravitational attraction over these regions reach $\sim 300 \text{ mGal}$.

Acknowledgments. Peter Vajda was partially supported by the VEGA grant agency under projects No. 2/0107/09 and 1/0461/09.

References

- Abramowitz M., Stegun I. A., 1972: Handbook of Mathematical Functions with Formulas, Graphs, and Mathematical Tables. New York, Dover Publications.
- Bassin C., Laske G., Masters G., 2000: The current limits of resolution for surface wave tomography in North America. EOS, Trans. AGU 81:F897.
- Cutnell J. D., Kenneth W. J., 1995: Physics, 3rd Edition, Wiley, New York.
- Hinze W. J., 2003: Bouguer reduction density, why 2.67? Geophysics, **68**, 5, 1559–1560.
- Huang J., Vaníček P., Pagiatakis S. D., Brink W., 2001: Effect of topographical density on the geoid in the Canadian Rocky Mountains. J. Geod., **74**, 805–815.
- Hunegnaw A., 2001: The effect of lateral density variation on local geoid determination. Bollettino di geodesia e scienze affini, **60**, 2, 125–144.
- Kaban M. K., Schwintzer P., Tikhotsky S. A., 1999: Global isostatic gravity model of the Earth. Geophys. J. Int., **136**, 519–536.
- Kaban M. K., Schwintzer P., 2001: Oceanic upper mantle structure from experimental scaling of V_s and density at different depths. Geophys. J. Int., **147**, 199–214.

- Kaban M. K., Schwintzer P., Artemieva I. M., Mooney W. D., 2003: Density of the continental roots: compositional and thermal contributions. *Earth Planet. Sci. Lett.*, **209**, 53–69.
- Kaban M. K., Schwintzer P., Reigber Ch., 2004: A new isostatic model of the lithosphere and gravity field. *J. Geod.*, **78**, 368–385, doi: 10.1007/s00190-004-0401-6.
- Kühtreiber N., 1998: Precise geoid determination using a density variation model. *Physics and Chemistry of the Earth*, **23**, 1, 59–63.
- Martinec Z., Vaníček P., Mainville A., Veronneau M., 1995: The effect of lake water on geoidal height. *Manusc. Geod.*, **20**, 193–203.
- Martinec Z., 1998: Boundary-value problems for gravimetric determination of a precise geoid. *Lecture Notes in Earth Science*, **73**, Springer-Verlag, Berlin-Heidelberg-New York.
- Moritz H., 1980: *Advanced physical geodesy*. Karlsruhe: Wichmann, Tunbridge, Eng., Abacus Press.
- Novák P., Vaníček P., Martinec Z., Veronneau M., 2001: Effects of the spherical terrain on gravity and the geoid. *J. Geod.*, **75**, 9-10, 491–504.
- Novák P., Grafarend E. W., 2005: The ellipsoidal representation of the topographical potential and its vertical gradient. *J. Geod.*, **78**, 11-12, 691–706.
- Novák P., 2010: High resolution constituents of the Earth gravitational field. *Surveys in Geophysics*, **31**, 1, 1–21, doi: 10.1007/s10712-009-9077-z.
- Novotný O., 1982: On the additional theorem for Legendre polynomials. *Travaux Geophysics*, **30**, 33–45.
- Peltier W. R., 2004: Global Glacial Isostasy and the Surface of the Ice-Age Earth: The ICE-5G (VM2) Model and GRACE, *Ann. Rev. Earth and Planet. Sci.*, **32**, 111–149.
- Ramillien G., 2002: Gravity/magnetic potential of uneven shell topography, *J. Geod.*, **76**, 139–149.
- Rummel R., Rapp R. H., Suenkel H., Tscherning C. C., 1988: Comparison of global topographic/isostatic models to the Earth's observed gravitational field. Report, **388**, The Ohio State University, Columbus, Ohio 43210-1247.
- Sjöberg L. E., 2004: The effect on the geoid of lateral topographic density variations. *J. Geod.*, **78**, 1-2, 34–39.
- Sun W., Sjöberg L. E., 2001: Convergence and optimal truncation of binomial expansions used in isostatic compensations and terrain corrections. *J. Geod.*, **74**, 627–636.
- Sünkel H., 1968: Global topographic-isostatic models. In: *Mathematical and numerical techniques in Physical geodesy* (Ed. Sünkel H.), *Lecture Notes in Earth Sciences*, **7**, Springer-Verlag, 417–462.
- Tenzer R., Vaníček P., Novák P., 2003: Far-zone contributions to topographical effects in the Stokes-Helmert method of the geoid determination. *Stud. Geoph. Geod.*, **47**, 3, 467–480.
- Tenzer R., Hamayun, Vajda P., 2008a: Global secondary indirect effects of topography, bathymetry, ice and sediments. *Contrib. Geophys. Geod.*, **38**, 2, 209–216.
- Tenzer R., Hamayun, Vajda P., 2008b: Global map of the gravity anomaly corrected for complete effects of the topography, and of density contrasts of global ocean, ice, and sediments. *Contrib. Geophys. Geod.*, **38**, 4, 357–370.

- Tenzer R., Hamayun, Vajda P., 2009a: Global maps of the step-wise topography corrected and crustal components stripped geoids using the CRUST 2.0 model. *Contrib. Geophys. Geod.*, **39**, 1, 1–17.
- Tenzer R., Hamayun, Vajda P., 2009b: Global maps of the CRUST 2.0 crustal components stripped gravity disturbances. *Journal Geophysical Research (Solid Earth)*, **114**, B05408, doi: 10.1029/2008JB006016.
- Tenzer R., Vajda P., Hamayun, 2009c: Global atmospheric corrections to the gravity field quantities. *Contrib. Geophys. Geod.*, **39**, 3, 221–236.
- Tenzer R., Vajda P., Hamayun, 2010: A mathematical model of the bathymetry-generated external gravitational field. *Contrib. Geophys. Geod.*, **40**, 1, 1–14.
- Timco G. W., Frederking R. M. W., 1996: A review of sea ice density. *Cold Regions Science and Technology*, **24**, 1, 1–6, doi:10.1016/0165-232X(95)00007-X.
- Tsoulis D., 1999: Spherical harmonic computations with topographic/isostatic coefficients. Reports in the series IAPG / FESG (ISSN 1437-8280), Rep., **3** (ISBN 3-934205-02-X), Institute of Astronomical and Physical Geodesy, Technical University of Munich.
- Tsoulis D., 2001: A Comparison between the Airy-Heiskanen and the Pratt-Hayford isostatic models for the computation of potential harmonic coefficients. *J. Geod.*, **74**, 9, 637–643, doi: 10.1007/s001900000124.
- van den Broeke M., 2008: Depth and density of the Antarctic firn layer. *Arctic, Antarctic, and Alpine Research*, **40**, 2, 432–438.
- Vaniček P., Najafi M., Martinec Z., Harrie L., Sjöberg L. E., 1995: Higher-degree reference field in the generalised Stokes-Helmert scheme for geoid computation. *J. Geod.*, **70**, 176–182.